CHEMISTRY OF MATERIALS
Article

Chem. Mater. **2010,** *22,* 4471–4483 4471
DOI:10.1021/cm1011795

Evidence of Intermediate-Range Order Heterogeneity in Calcium Aluminosilicate Glasses

Mette Moesgaard,[†] Ralf Keding,[†] Jørgen Skibsted,[‡] and Yuanzheng Yue*,[†]

[†]*Section of Chemistry, Aalborg University, DK-9000 Aalborg, Denmark, and* [‡]*Instrument Centre for Solid-State NMR spectroscopy and Interdisciplinary Nanoscience Center (iNANO), Department of Chemistry, Aarhus University, DK-8000 Aarhus, Denmark*

Received April 27, 2010. Revised Manuscript Received June 16, 2010

The intermediate-range order in peralkaline calcium aluminosilicate glasses is explored by two different models using solid-state ^{29}Si MAS NMR spectra as the main experimental basis. The two modeling approaches describe the spatial arrangement of the tetrahedral SiO_4 and AlO_4 units, that is, the intermediate-range order (IRO), assuming either a random distribution of structural units or a hierarchy in the IRO. The hierarchy creates a quasi-heterogeneous distribution of the structural units. Two series of calcium aluminosilicate glasses (five glasses for each) are chosen for the present study, compositions of which vary along the join between the anorthite-wollastonite-gehlenite eutectic point and anorthite-wollastonite-tridymite point, and parallel to the join. The validity of the two modeling approaches is examined by simulation of the frequency and intensity distributions observed in the ^{29}Si MAS NMR spectra of the 10 glasses using a sum of resonances predicted for the different types of structural units. The results clearly reveal that the ^{29}Si MAS NMR spectra support the quasi-heterogeneous IRO for the 10 glasses, since this approach gives a satisfactory fit to the experimental spectra. In contrast, simulations based on the model of random IRO cannot reproduce the ^{29}Si NMR spectra in a satisfactory manner. The observed hierarchy in the IRO may also explain the compositional dependence of both viscous behavior of the melts and the stability of the 10 glasses.

1. Introduction

The physical and chemical properties of a glass are determined mainly by its microstructure (hereafter called structure), which to a large extent depends on its chemical composition. In general, the characterization and understanding of the structure of crystalline materials have been established more thoroughly as compared to that of noncrystalline materials (i.e., glasses), reflecting the lack of long-range structural order in glasses which prevents the application of conventional structural tools such as X-ray diffraction techniques. Nevertheless, a substantial progress in our understanding of glass structures has been achieved in the past century[1−4] and in particular in recent years because of the rapid technical improvements of experimental tools such as EXAFS,[5,6] NMR spectroscopy,[5,7,8] and molecular dynamics simulations.[9] Using these tools, several aspects of both the short-range and the intermediate-range structure of silicate glasses have been clarified. However, some puzzles still remain unsolved, especially, about the role of heterogeneity in the overall structural network.

Much effort has been devoted to determination of the topological arrangements of Al ions in aluminosilicate glasses, for example, the coordination number of Al, the bond-angle distribution, the linkage of AlO_x to alkali or alkaline earth ions, and the fulfillment of the aluminum avoidance principle.[7,9−15] Using different solid-state NMR techniques, Stebbins and co-workers[8,10−14] have investigated the structure of aluminosilicate glasses primarily along "charge compensated" joins, along which the total charge of the network modifying ions equals that of the AlO_2 units (e.g., $SiO_2-NaAlO_2$ and $SiO_2-CaAl_2O_4$ systems). Using Raman spectroscopy, Mysen and co-workers[16−18] have performed careful structural investigations of various "charge compensated" and peralkaline aluminosilicates. These results are the fundamental basis for the structural investigations of the calcium aluminosilicate (CAS) glasses presented in this work. However, the compositions of the

*To whom correspondence should be addressed. E-mail: yy@bio.aau.dk. Phone: +45 99408522. Fax: +45 96350558.

(1) Warren, B. E. *J. Am. Ceram. Soc.* **1934**, *17*, 249.
(2) Wright, A. C.; Leadbetter, A. J. *Phys. Chem. Glasses* **1976**, *17*, 122.
(3) Farnan, I.; Grandinetti, P. J.; Baltisberger, J. H.; Stebbins, J. F.; Werner, U.; Eastman, M. A.; Pines, A. *Nature* **1992**, *358*, 31.
(4) Gaskell, P. H. *J. Non-Cryst. Solids* **1997**, *222*, 1.
(5) Greaves, G. N.; Sen, S. *Adv. Phys.* **2007**, *56*, 1.
(6) Brown, G. E. J.; Farges, F.; Calas, G. *Rev. Miner.* **1995**, *32*, 317.
(7) Eckert, H. *Progr. NMR Spectrosc.* **1992**, *24*, 159.
(8) Lee, S. K.; Stebbins, J. F. *Am. Mineral.* **1999**, *84*, 937.
(9) Du, J.; Cormack, A. N. *J. Non-Cryst. Solids* **2004**, *349*, 66.
(10) Lee, S. K.; Stebbins, J. F. *J. Phys. Chem. B* **2000**, *104*, 4091.
(11) Stebbins, J. F.; Lee, S. K.; Oglesby, J. V. *Am. Mineral.* **1999**, *84*, 983.
(12) Lee, S. K.; Stebbins, J. F. *J. Non-Cryst. Solids* **2000**, *270*, 260.
(13) Murdoch, J. B.; Stebbins, J. F.; Carmichael, I. S. E. *Am. Mineral.* **1985**, *70*, 332.
(14) Stebbins, J. *Nature* **1987**, *330*, 13.
(15) De Jong, B. H. W. S.; Brown, G. E. *Geochim. Cosmochim. Acta* **1980**, *44*, 491.
(16) Mysen, B. *Contrib. Mineral. Petrol.* **1997**, *127*, 104.
(17) Mysen, B. O. *Am. Mineral.* **1990**, *75*, 120.
(18) Mysen, B. O.; Virgo, D.; Kushiro, I. *Am. Mineral.* **1981**, *66*, 678.

Published on Web 07/15/2010

glasses in the present study deviate from those in previous investigations of aluminosilicate glasses as the glasses in this work generally possess relatively higher contents of both non-bridging oxygen (NBO) anions and Al^{3+} cations.

In this work we investigate the structure of peralkaline glasses within the CAS system. During the optimization of the chemical composition for a technical glass, with a similar composition as the CAS glasses investigated in this study, we found in a recent study a striking compositional dependence on both the glass forming ability and the melt fragility of the CAS melts.[19] To understand this behavior in more detail, it is necessary to characterize the structural changes that occur when the composition is modified, since the glass forming ability is dictated by the topological arrangement and the chemical bonding strength of glasses. In addition, investigations of the structure for the CAS system is particularly interesting since the majority of magmatic compositions and several technical glasses belong to aluminosilicate systems.[20,21]

In the present study we establish two different structural models for the intermediate-range order (IRO) and investigate their applicability to describe the distribution of structural units within two series of glasses, each including five different compositions. The IRO is defined as the structure extending beyond nearest neighbors (NN) within the glass. In one approach, a random spatial rearrangement of structural units is assumed, referred to as the "random IRO" (R-IRO) model. The other model employs a hierarchy in the intermediate-range order, resulting in a quasi-heterogeneous distribution of structural units and is thus denoted as the "quasi-heterogeneous IRO" (QH-IRO) model. The contents of the different structural units in the 10 glasses are derived from the two models using the chemical compositions of the glasses along with their solid-state ^{29}Si MAS NMR spectra. The validity of the models is evaluated by their ability to simulate the intensity and frequency distributions in the ^{29}Si MAS NMR spectra.

^{29}Si MAS NMR is a well-documented powerful tool for structural studies of aluminosilicates.[22−25] It is widely used as the isotropic ^{29}Si chemical shift ($\delta(^{29}Si)$) depends on both the degree of polymerization of SiO_4 tetrahedra and the presence of Al in the second coordination sphere to Si. However, simultaneous changes in the content of both the network modifying ions and the network forming Al ions may complicate the interpretation of single-pulse ^{29}Si MAS NMR experiments. In such cases, supporting information may be obtained from two-dimensional ^{17}O and ^{27}Al triple-quantum (3Q) MAS NMR experiments, where ^{17}O requires the use of isotopically enriched samples.[10,12] In this work the structural modeling based on the chemical composition of the glasses allows extraction of new important information about the IRO from the single pulse ^{29}Si MAS NMR experiments.

Table 1. Oxide Compositions (mol %) for the 10 CAS Glasses

	glass[a]	SiO_2	Al_2O_3	CaO	Ca_{excess}[b]
series 1	$C_{26}A_9S_{65}$	64.9	9.3	25.8	16.6
	$C_{30}A_{10}S_{60}$	59.9	10.0	30.1	20.0
	$C_{34}A_{11}S_{55}$	54.7	10.9	34.4	23.5
	$C_{39}A_{12}S_{49}$	49.6	11.7	38.7	27.1
	$C_{43}A_{13}S_{44}$	44.4	12.5	43.1	30.6
series 2	$C_{23}A_{15}S_{62}$	61.6	14.9	23.4	8.0
	$C_{26}A_{16}S_{58}$	57.8	15.8	26.3	10.5
	$C_{31}A_{17}S_{52}$	51.9	16.8	31.3	13.0
	$C_{33}A_{19}S_{48}$	48.1	18.9	33.0	15.5
	$C_{38}A_{19}S_{43}$	42.7	19.3	38.0	18.0

[a] The sample names refer to the actual molar compositions determined by wet chemical analysis. [b] Ca_{excess} is the amount of Ca^{2+} ions which is not used for charge balancing the Al^{3+} ions.

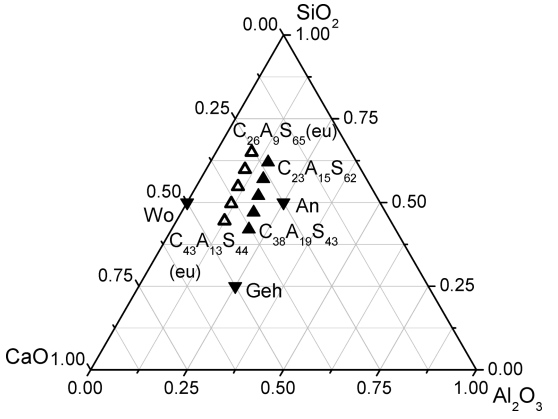

Figure 1. Graphical representation of the compositions for the 10 glasses (upward triangles) in the CAS ternary phase diagram (mol %). The open triangles represent series 1 (i.e., $C_{26}A_9S_{65}$ to $C_{43}A_{13}S_{44}$) with the two end members being the eutectic compositions of An-Wo-Geh and An-Wo-Tri, while series 2 ($C_{23}A_{15}S_{62}$−$C_{38}A_{19}S_{43}$) is illustrated by the solid upward triangles. The downward triangles correspond to the compositions for the mineral phases wollastonite, anorthite, and gehlenite.

2. Experimental Section

The glasses are divided into two series of systematic compositional variations and are placed in the vicinity of the eutectic compositions for anorthite-wollastonite-gehlenite (An-Wo-Geh) and anorthite-wollastonite-tridymite (An-Wo-Tri). The compositions of the 10 glasses are summarized in Table 1 while their location in the ternary CAS system is illustrated in Figure 1. The sample names of the glasses refer to the molar oxide composition determined from wet chemical analysis with C, A, and S representing CaO, Al_2O_3, and SiO_2, respectively

The glasses were synthesized by melting the batch in a $Pt_{90}Rh_{10}$ crucible in an electric furnace (model SF6/17 Entech, Ängelholm, Sweden) in atmospheric air. The individual compositions were obtained by mixing reagent-grade chemicals of SiO_2, Al_2O_3, and $CaCO_3$. A two-step melting process was carried out to obtain a homogenized glass. First, the batch was melted at 1823 K and kept at this temperature for 2 h. Subsequently, the melt was quenched in water to get shattered pieces. The shattered glass was melted again at 1823 K for 2 h and cast on a graphite plate. The chemical compositions of the resulting glasses (Table 1) were determined by standard wet chemical analysis at the Cement and Concrete Laboratory of the Aalborg Portland Group, Aalborg, Denmark.

(19) Moesgaard, M.; Yue, Y. Z. *J. Non-Cryst. Solids* **2009**, *355*, 867.
(20) Mysen, B. O.; Richet, P. *Silicate glasses and melts properties and structure*; Elsevier B.V.: Amsterdam, 2005.
(21) Stebbins, J. F.; Xu, Z. *Nature* **1997**, *390*, 60.
(22) Lippmaa, E.; Mägi, M.; Samoson, A.; Engelhardt, G.; Grimmer, A. R. *J. Am. Chem. Soc.* **1980**, *102*, 4889.
(23) Mägi, M.; Lippmaa, E.; Engelhardt, G.; Grimmer, A. R. *J. Phys. Chem.* **1984**, *88*, 1518.
(24) Klinowski, J. *Progr. NMR Spectrosc.* **1984**, *16*, 237.
(25) Lippmaa, E.; Mägi, M.; Samoson, A.; Tarmak, M.; Engelhardt, G. *J. Am. Chem. Soc.* **1981**, *103*, 4992.

The ^{29}Si MAS NMR spectra were recorded at 59.1 MHz on a Varian INOVA-300 (7.05 T) spectrometer, using a home-built CP/MAS probe for 7 mm outer diameter (o.d.) rotors. The powder samples, ground to a fineness below 75 μm, were packed in 7 mm partially sintered zirconia (PSZ) rotors (220 μL sample volume) and spun at 7.0 kHz. The experiments employed a radio frequency (rf) field strength of $\gamma B_1/2\pi \approx 40.0$ kHz, a pulse width of 3.0 μs ($\sim$45° flip angle), a 120 s repetition delay, and 1000−1400 scans. The ^{27}Al MAS NMR spectra were recorded at 104.2 and 156.3 MHz on Varian INOVA-400 (9.39 T) and INOVA-600 (14.09 T) spectrometers using home-built CP/MAS probes for 5 and 4 mm o.d. rotors, respectively. The 9.39 T spectra employed a spinning speed of 12.0 kHz, a 0.5 μs excitation pulse for $\gamma B_1/2\pi \approx 60.0$ kHz, a 2 s relaxation delay, and typically 6000 scans. The 14.09 T spectra used a spinning speed of 13.0 kHz, a 0.5 μs excitation pulse for $\gamma B_1/2\pi \approx 60.0$ kHz, a 2 s relaxation delay, and 1400−2100 scans. The ^{27}Al and ^{29}Si isotropic chemical shifts are reported relative to a 1.0 M aqueous solution of $AlCl_3 \cdot 6H_2O$ and neat tetramethyl silane (TMS), respectively.

The simulations and optimizations to the ^{29}Si MAS NMR spectra have been performed using the scaled Levenberg−Marquardt non-linear least-squares algorithm[26] included in the program QtiPlot 0.9.6.[27] A tolerance of 10^{-4} is used for the simulations.

3. Theoretical Approach

3.1. Distribution of Bridging and Non-Bridging Oxygen. A classical and commonly used model for silicate glass structures is the continuous random network (CRN) model proposed by Zachariasen.[28] The CRN model describes the glass structure as a three-dimensional network of corner-linked low-valence cation-oxygen polyhedra where the introduction of modifying oxides to the glass leads to the formation of NBOs randomly distributed within the three-dimensional network. On the basis of the CRN model, Greaves[29] has proposed the modified random network (MRN) model where different sizes of the network-forming and network-modifying polyhedra result in a micro segregation of the two structural units. This creates regions of modifier rich channels and other regions rich in more highly polymerized network-forming polyhedra.[5,9,30]

All glasses investigated in this work are peralkaline, in which both Si and Al act as network forming components. The excess Ca ions (Ca_{excess}), which are not involved in the charge balance of Al^{3+} ions, serve to charge balance the NBOs that are created by the presence of excess oxide ions. The first step in the description of the structure is to model the distribution of the various network forming (Si,Al)O_4 Q^n units (n is the number of bridging oxygens (BOs) linked to the network former). A preference of Al for fully polymerized Q^4 sites in peralkaline aluminosilicates has been reported in several studies,[17,18,20,31−33] that is, no NBOs are linked directly to Al. This preference is found to increase with increasing Si/Al ratio, and for Si/Al > 1 the content of Al-NBO is reported to be insignificant.[31−33] For the samples studied in this work, the Si/Al ratio varies between 1.1 ($C_{38}A_{19}S_{43}$) and 3.5 ($C_{26}A_9S_{65}$), and Al is assigned solely to Q^4 units, implying that excess CaO will create NBOs associated with Si only.

Despite several investigations, inconsistencies in the description of the Q^n distribution of SiO_4 units in silicate glasses still remain within the glass community. Generally, two models are considered, that is, the binary model and the random model.[5,34−36] The former assumes the existence of only two different Si(Q^n) units for a specific glass composition, the argument being that repulsive forces between the modifying ions prevent these ions from entering a site adjacent to Si in, for example, a Q^2 unit until no other Q^3 units are present. On the other hand, the random model assumes a statistical distribution of Q^n units for n = 0−4. The two models represent extreme situations and thus, Q^n distributions lying in between these two situations have been reported by several authors.[5,16,20,35,37,38] For example, ^{29}Si MAS NMR studies of binary alkali silicate systems have indicated the presence of three different Q^n units[34,37−39] and thereby that the randomness is larger than predicted by the binary model although still less than predicted by the random model. It has also been reported that a large field strength of the modifying ions increases the structural disorder.[13,20,31,35] From the relatively large field strength of calcium ions, the CAS glasses investigated in this work are expected to contain a certain degree of randomness deviating further from the binary model as compared to the alkali silicate systems as evidenced from investigations of such systems.[13,40] Hence, the random model is chosen to describe the distribution of Q^n units in the CAS glasses. In this model, the probability (p) that a randomly chosen Si−O bond includes a NBO is calculated as the ratio between the number of NBOs divided by the total number of bonds (NBO + BO):

$$p = \frac{\mathrm{NBO}}{\mathrm{NBO} + \mathrm{BO}} = \frac{2Ca_{excess}}{Z \cdot \mathrm{Si}} \qquad (1)$$

Here, Ca_{excess} and Si are the numbers of the excess calcium ions and the number of glass forming Si ions, respectively, while Z is the coordination number of the network former, that is, $Z = 4$. Using the p value obtained for the individual

(26) Marquardt, D. W. *J. Soc. Industr. Appl. Math.* **1963**, *11*, 31.
(27) *Qtiplot*; http://soft.proindependent.com/install.html.
(28) Zachariasen, W. H. *J. Am. Chem. Soc.* **1932**, *54*, 3841.
(29) Greaves, G. N. *J. Non-Cryst. Solids* **1985**, *71*, 203.
(30) Gedeon, O.; Liska, M.; Machacek, J. *J. Non-Cryst. Solids* **2008**, *354*, 1133.
(31) Merzbacher, C. I.; Sherriff, B. L.; Hartman, J. S.; White, W. B. *J. Non-Cryst. Solids* **1990**, *124*, 194.
(32) Allwardt, J. R.; Lee, S. K.; Stebbins, J. F. *Am. Mineral.* **2003**, *88*, 949.
(33) Lee, S. K.; Stebbins, J. F. *Geochim. Cosmochim. Acta* **2006**, *70*, 4275.
(34) Stebbins, J. F. *J. Non-Cryst. Solids* **1988**, *106*, 359.
(35) Buckermann, W. A.; Müller-Warmuth, W.; Frischat, G. H. *Glastech. Ber.* **1992**, *65*, 18.
(36) Avramov, I.; Rüssel, C.; Keding, R. *J. Non-Cryst. Solids* **2003**, *324*, 29.
(37) Emerson, J. F.; Stallworth, P. E.; Bray, P. J. *J. Non-Cryst. Solids* **1989**, *113*, 253.
(38) Maekawa, H.; Maekawa, T.; Kawamura, K.; Yokokawa, T. *J. Non-Cryst. Solids* **1991**, *127*, 53.
(39) Schramm, C. M.; De Jong, B. H. W. S.; Parziale, V. E. *J. Am. Chem. Soc.* **1984**, *106*, 4396.
(40) Schneider, E.; Stebbins, J. F.; Pines, A. *J. Non-Cryst. Solids* **1987**, *89*, 371.

Table 2. Calculated Distributions of Si(Q^n) Units for the 10 Glasses Assuming a Random Distribution of NBOs[a]

glass	Q^0	Q^1	Q^2	Q^3	Q^4
$C_{26}A_9S_{65}$	0	0	7.42	33.87	57.96
$C_{30}A_{10}S_{60}$	0	1.56	11.66	38.65	48.05
$C_{34}A_{11}S_{55}$	0	3.12	17.10	41.60	37.96
$C_{39}A_{12}S_{49}$	0	5.91	23.62	41.96	27.96
$C_{43}A_{13}S_{44}$	1.41	10.71	30.59	38.82	18.47
$C_{23}A_{15}S_{62}$	0	0	2.19	21.13	76.59
$C_{26}A_{16}S_{58}$	0	0	4.20	27.57	67.94
$C_{31}A_{17}S_{52}$	0	0	7.18	33.50	58.62
$C_{33}A_{19}S_{48}$	0	1.50	11.38	38.41	48.64
$C_{38}A_{19}S_{43}$	0	3.09	17.01	41.58	38.11

[a] The fractions are given as molar percents. "0" indicates that the unit accounts for less than 1% of the SiO_4 units in the sample. The distributions are calculated using eqs 1 and 2.

compositions, the molar fraction $x(Q^n)$ for each of the Si(Q^n) units can be calculated by combinatorics assuming a statistical distribution:

$$x(\mathrm{Si}(Q^n)) = \frac{Z!}{n!(Z-n)!}(1-p)^n p^{Z-n} = \frac{4!}{n!(4-n)!}(1-p)^n p^{4-n} \quad (2)$$

Introduction of Al into a silicate glass enhances the structural disorder since the randomness is found to increase as the Si/Al ratio decreases.[10,16,34] This also means that use of the random model is reasonable for describing the distribution of different Q^n units in aluminosilicates. Table 2 lists the distributions of Si(Q^n) units for the 10 glasses obtained from eqs 1 and 2. The molar fraction of Si(Q^n) units of < 1% is neglected in the modeling of the ^{29}Si MAS NMR spectra, and thus, the presence of Q^0 units is neglected for all glasses except $C_{43}A_{13}S_{44}$ for which the fraction of Q^0 accounts for 1.41% of the structural units.

3.2. Al Avoidance Principle. The relative distribution of SiO_4 and AlO_4 units in the glass network is described in terms of the Si nuclei and the distribution of Al in the second coordination sphere of Si. Thus, the modeling approach provides no information on the identity of the network former linked to the AlO_4 tetrahedra in the following coordination spheres, that is, the Al avoidance principle[41] is not directly considered. The only assumption made is that all the Al ions are available for linking with SiO_4 tetrahedra, that is, no formation of large clusters of Al structural units is expected. The Al avoidance principle has previously been deduced from experimental observations,[13] and it is supported by theoretical calculations showing that the Al−O−Al linkages are energetically less favorable than Si−O−Si and Si−O−Al linkages.[15] However, it has also been reported that the Al avoidance principle is not fully obeyed within aluminosilicate glasses.[8,10−14] The degree of Al avoidance is derived from the equilibrium constant of the reaction, 2(Al−O−Si) ↔ (Si−O−Si) + (Al−O−Al),[11] and an Al avoidance degree of 1 corresponds to complete Al avoidance whereas a value of 0 denotes a random distribution of network forming Si and Al units. It is estimated that the degree of Al avoidance for CAS glasses positioned on the meta-aluminous limit is about 0.85.[8,10−14]

The fulfillment of the Al avoidance principle in the present approach depends on the Si/Al ratio and the content of NBOs linked to Si. When the total number of BOs bound to Si is larger than the total number of BOs bound to Al, the Al avoidance principle can be fulfilled. This is the case for all glasses except $C_{38}A_{19}S_{43}$ for which at least 17% of Al is expected to be present in Al−O−Al linkages. The fulfillment of the Al avoidance principle in the two IRO modeling approaches is discussed later.

3.3. Random Intermediate-Range Order (R-IRO) Model. The first approach for modeling of the intermediate-range order is based on the principles of the CRN model. The structure beyond the nearest neighbors is thus described by a random distribution of Al around the SiO_4 tetrahedra. This distribution is assumed to follow similar statistical principles as for the NBOs around Si. The probability that a randomly picked Si-BO unit is linked to Al is initially calculated as the ratio between the content of Al and the total content of network forming cations (Si + Al) (Similar approach as eq 1). Using this probability, the fraction of each Si($Q^{ni}(m_i\mathrm{Al})$) unit (m is the number of Al in the second coordination sphere to Si) is calculated as listed in Table 3 using the algorithm of eq 2. Again, structural units accounting for less than 1% of the sample are neglected. The number of non-negligible units increases within each series, when the content of both NBO and Al increases from $C_{26}A_9S_{65}$ to $C_{43}A_{13}S_{44}$ (series 1) and from $C_{23}A_{15}S_{62}$ to $C_{38}A_{19}S_{43}$ (series 2). For $C_{26}A_9S_{65}$, 9 different structural units exist whereas 13 non-negligible units are found for $C_{43}A_{13}S_{44}$. In the other series, $C_{23}A_{15}S_{62}$ has 7 non-negligible units while $C_{38}A_{19}S_{43}$ are found to include 14 different structural units.

3.4. Quasi-Heterogeneous Intermediate-Range Order (QH-IRO) Model. The QH-IRO model is based on the principles of the modified random network (MRN) model[29] which predicts clustering of NBOs within silicate glasses. For the glasses studied in the present work, clustering of NBOs results in highly polymerized regions of alternating SiO_4 and AlO_4 tetrahedra as well as highly depolymerized regions containing only a minor content of Al. This clustering creates concentration fluctuations within the glasses, which have been reported for several multicomponent oxide glasses[42−46] and is ascribed to the existence of chemical heterogeneities in the range of ∼1−3 nm. The existence of such an IRO hierarchy is supported by experimental observations from Raman spectroscopy, light scattering, and small-angle X-ray scattering studies.[43−45] Furthermore, a preferential bonding of Al to fully polymerized SiO_4 tetrahedra has been reported,[31,47,48] which supports the existence of nanometric spatial regions with different heterogeneities within the

(41) Loewenstein, W. *Am. Mineral.* **1954**, *39*, 92.
(42) Martinez, V.; Jurdyc, A. M.; Vouagner, D.; Martinet, C.; Champagnon, B. *J. Non-Cryst. Solids* **2005**, *351*, 2421.
(43) Conradt, R. *J. Non-Cryst. Solids* **2004**, *345&346*, 16.
(44) Mauro, J. C.; Uzun, S. S.; Bras, W.; Sen, S. *Phys. Rev. Lett.* **2009**, *102*, 155506.
(45) Moynihan, C. T.; Schroder, J. *J. Non-Cryst. Solids* **1993**, *160*, 52.
(46) Champagnon, B.; Wondraczek, L.; Deschamps, T. *J. Non-Cryst. Solids* **2009**, *355*, 712.
(47) Domine, F.; Piriou, B. *Am. Mineral.* **1986**, *71*, 38.
(48) Hess, P. C.; Wood, M. I. *Contrib. Mineral. Petrol.* **1982**, *81*, 103.

Table 3. Calculated Distributions of Si($Q^{ni}(m_i$Al)) Units for the 10 Glasses Obtained by the R-IRO Model[a]

glass	Q^0	Q^1(1Al)	Q^1(0Al)	Q^2(2Al)	Q^2(1Al)	Q^2(0Al)
$C_{26}A_9S_{65}$	0	0	0	0	2.56	4.49
$C_{30}A_{10}S_{60}$	0	0	1.17	0	4.39	6.53
$C_{34}A_{11}S_{55}$	0	0	2.24	1.38	6.95	8.77
$C_{39}A_{12}S_{49}$	0	1.89	4.02	2.42	10.28	10.93
$C_{43}A_{13}S_{44}$	1.41	3.85	6.86	3.95	14.09	12.55
$C_{23}A_{15}S_{62}$	0	0	0	0	0	0
$C_{26}A_{16}S_{58}$	0	0	0	0	1.94	1.70
$C_{31}A_{17}S_{52}$	0	0	0	1.16	3.45	2.56
$C_{33}A_{19}S_{48}$	0	0	0	2.24	5.62	3.52
$C_{38}A_{19}S_{43}$	0	1.51	1.58	4.05	8.50	4.46
i^b	1	2	3	4	5	6
$n_i{}^b$	0	1	1	2	2	2
$m_i{}^b$	0	1	0	2	1	0

	Q^3(3Al)	Q^3(2Al)	Q^3(1Al)	Q^3(0Al)	Q^4(4Al)	Q^4(3Al)	Q^4(2Al)	Q^4(1Al)	Q^4(0Al)
$C_{26}A_9S_{65}$	0	3.89	13.65	15.96	0	1.97	10.37	24.24	21.25
$C_{30}A_{10}S_{60}$	0	5.49	16.34	16.21	0	2.29	10.22	20.27	15.08
$C_{34}A_{11}S_{55}$	0	7.21	18.17	15.27	0	2.49	9.42	15.83	9.98
$C_{39}A_{12}S_{49}$	1.37	8.76	18.63	13.21	0	2.49	7.94	11.25	5.98
$C_{43}A_{13}S_{44}$	1.80	9.64	17.18	10.20	0	2.20	5.88	6.98	3.11
$C_{23}A_{15}S_{62}$	0	4.54	9.39	6.47	0	7.16	22.19	30.57	15.80
$C_{26}A_{16}S_{58}$	1.32	6.95	12.18	7.12	1.18	8.29	21.80	25.49	11.18
$C_{31}A_{17}S_{52}$	2.18	9.72	14.44	7.15	1.54	9.12	20.34	20.14	7.48
$C_{33}A_{19}S_{48}$	3.36	12.62	15.82	6.61	1.89	9.46	17.78	14.86	4.66
$C_{38}A_{19}S_{43}$	4.83	15.20	15.96	5.59	2.16	9.06	14.27	9.99	2.62
i^b	7	8	9	10	11	12	13	14	15
$n_i{}^b$	3	3	3	3	4	4	4	4	4
$m_i{}^b$	3	2	1	0	4	3	2	1	0

[a] The contents are given as molar percentages where "0" indicates that the unit accounts for less than 1% of the sample. [b] Index numbers used for the different $\delta(Q^{ni}(m_i$Al)) units in eqs 3 and for the deconvolution of the ^{29}Si NMR resonances. The relative intensities for the individual resonances (a_i) are the molar fractions listed in the rows above for the different glasses.

Table 4. Calculated Distributions of Si($Q^{ni}(m_i$Al)) Units Obtained by the HQ-IRO Model[a]

	Q^0	Q^1(0Al)	Q^2(2Al)	Q^2(0Al)	Q^3(3Al)	Q^3(0Al)	Q^4(4Al)	Q^4(0Al)
$C_{26}A_9S_{65}$	0	0	0	7.42	0	33.87	28.51	29.45
$C_{30}A_{10}S_{60}$	0	1.56	0	11.66	0	38.65	33.60	14.45
$C_{34}A_{11}S_{55}$	0	3.12	0	17.10	1.70	39.90	37.96	0
$C_{39}A_{12}S_{49}$	0	5.91	0	23.62	19.06	22.90	27.96	0
$C_{43}A_{13}S_{44}$	1.41	10.71	0	30.59	37.65	1.17	18.47	0
$C_{23}A_{15}S_{62}$	0	0	0	2.19	0	21.13	48.39	28.20
$C_{26}A_{16}S_{58}$	0	0	0	4.20	0	27.57	57.02	10.93
$C_{31}A_{17}S_{52}$	0	0	0	7.18	8.69	24.81	58.62	0
$C_{33}A_{19}S_{48}$	0	1.50	0	11.38	31.15	7.26	48.64	0
$C_{38}A_{19}S_{43}$	0	3.09	15.55	1.46	41.58	0	38.11	0

[a] Quantities in molar percents. "0" indicates that the unit accounts for less than 1% of the sample.

glasses. This quasi-heterogeneous nature of the distribution of structural units is most likely found for network modifying ions with a low positive charge density as these ions have only a small stabilizing effect on NBOs and AlO_4 tetrahedra linked to the same SiO_4 tetradedron.[31,47]

For the fully polymerized regions, a structure of alternating SiO_4-AlO_4 units is assumed. For $C_{26}A_9S_{65}$, $C_{30}A_{10}S_{60}$, $C_{23}A_{15}S_{62}$, and $C_{26}A_{16}S_{58}$, the Al content is sufficiently low, that is, Al(Q^4) < Si(Q^4) (in molar fractions), to assign all Al to these fully polymerized regions, thus obeying the Al avoidance principle. For the other six glasses the remaining Al, which is not part of the fully polymerized regions, that is, Al(Q^4)−Si(Q^4) (in molar fractions), is assigned to Si(Q^3(3Al)) units, since a Si(Q^3) with a neighboring Al is more stable than a Si(Q^2) unit with an Al neighbor. Again a 1:1 ratio of Si and Al is assumed for the Si(Q^3(3Al)) units, resulting in the Al-avoidance principle being broken for these regions. For the glass with the highest Al content ($C_{38}A_{19}S_{43}$), Al must in addition be assigned to Si(Q^2) units. The distribution of Si($Q^{ni}(m_i$Al)) units obtained from the HQ-IRO model is given in Table 4, which shows that the spatial intermediate-range arrangement of the glasses is described in terms of 4−6 different structural units. This contrasts the R-IRO model which predicts the presence of up to 14 different structural units (Table 3).

3.5. Comparison of the Models with ^{29}Si MAS NMR Spectra. The distribution of the Si($Q^{ni}(m_i$Al)) units, predicted for the 10 glasses from the two different models,

is compared with experimental ^{29}Si MAS NMR spectra of the glasses, providing information on the validity of the two different models in the description of the intermediate-range structure of the CAS glasses. The observed chemical shifts, $\delta(^{29}\mathrm{Si})$, for aluminosilicates depend on both the degree of polymerization of SiO_4 tetrahedra and the number of Al in their second coordination sphere. The ^{29}Si resonances observed experimentally are the sum of subpeaks originating from different SiO_4 environments where the subpeak area is proportional to the molar fraction of the individual Si(Q^{ni}-(m_iAl)) units. Thus, rather broad ^{29}Si resonances are expected since the models predict a range of different structural environments for each glass composition. The molar fractions for the individual Si(Q^{ni}(m_iAl)) units are determined by the structural models and summarized in Tables 3 and 4. During the modeling process the intensities of the subpeaks are constrained to match the molar fraction predicted by models.

For tetrahedrally coordinated Si in crystalline as well as amorphous silicates and aluminosilicates $\delta(^{29}\mathrm{Si})$ ranges from −60 to −120 ppm. This chemical shift region is split into smaller subregions, depending on the degree of polymerization of SiO_4 units. Fully polymerized Q^4 units exhibit chemical shifts in the range −100 to −120 ppm, and the introduction of a NBO lowers the shielding of the ^{29}Si nucleus by 5−10 ppm for each NBO,[22−24] resulting in characteristic shifts toward higher frequency for Q^3, Q^2, Q^1, and Q^0 SiO_4 tetrahedra. Furthermore, the replacement of a Si−O−Si by a Si−O−Al bond results in a similar shift (∼5 ppm) toward higher frequency,[8,22,24,25] preventing an unambiguous distinction of different Si(Q^{ni}(m_iAl)) units from the chemical shifts alone, for example, a Si(Q^4(2Al)) unit may exhibit the same chemical shift as a Q^3(0Al) SiO_4 tetrahedron.

To test the validity of the R-IRO and HQ-IRO models, the ^{29}Si MAS NMR spectra are deconvolved using a sum of Gaussian shaped resonances corresponding to the different types of Si(Q^{ni}(m_iAl)) units with relative intensities equal to the molar fractions predicted by the models (Tables 3 and 4).

$$f(x) = \sum_{i=1}^{15} \frac{a_i}{w \cdot \sqrt{\pi/2}} \exp\left[\frac{-2(x-x_{0i})^2}{w^2}\right] = \sum_{i=1}^{15} \frac{a_i}{w \cdot \sqrt{\pi/2}} \exp\left[\frac{-2(x-\delta(Q^{n_i}(m_i\mathrm{Al})))^2}{w^2}\right] \quad (3)$$

Thus, the ^{29}Si NMR resonances are described as a sum of Gaussian distributions (eq 3) where a_i is the relative area (i.e., the molar fraction) for a given structural unit and x_{0i} is the center of the resonance corresponding to the chemical shift $\delta(Q^{ni}(m_i\mathrm{Al}))$. During the deconvolutions a_i is assumed to have a constant value, corresponding to the values listed in Tables 3 and 4. The relation between i, n_i, and m_i for the different $\delta(Q^{ni}(m_i\mathrm{Al}))$ units are given by the last three rows in Table 3. The line width w is equal to 2σ, where σ is the standard deviation, and the relation between w and the full width at half-maximum (FWHM) is FWHM $= 2\sigma(2\ln 2)^{1/2} \approx 1.18w$. FWHM is expected to be of the order of ∼10 ppm for glasses, which is approximately 1 order of magnitude larger than the line widths observed for crystalline samples with similar compositions.[8,49] The increased line width observed for amorphous samples is caused by the distribution of bond angles and atomic distances present in these materials. The line width is assumed to be constant for all samples in the deconvolutions, which is considered a reasonable approximation, taking into account that the different glasses are synthesized under nearly identical conditions, that is, similar cooling rates, using the same starting materials. Thus, all 10 glasses are expected to exhibit similar bond-angle and atomic distance distributions. The line width is additionally dependent on the chemical environment of the Si nuclei. However, the broadening caused by different atoms in the first and second coordination spheres to Si is expected to be of minor importance for the glasses as compared to similar crystalline materials. The reason for this is that the resonances are already broadened because of the bond angle and atomic distance distributions within the glass. Furthermore, line broadening from ^{29}Si−^{29}Si dipolar interactions is negligible because of the low ^{29}Si natural abundance while heteronuclear ^{27}Al− ^{29}Si dipolar couplings and ^{29}Si chemical shift anisotropies are efficiently averaged out by magic-angle spinning. The usage of a constant line width within the modeling is discussed in greater detail later. The dependencies of chemical shift on the degree of polymerization of SiO_4 tetrahedra (n: the number of BO linked to Si) and on the incorporation of Al in the second coordination sphere (m: the number of Al) are assumed to be additive, that is, the chemical shift for a Q^{ni}(m_iAl) unit can be expressed by

$$x_{0i} = \delta(Q^{n_i}(m_i\mathrm{Al})) = \delta(Q^4(0\mathrm{Al})) + (4-n_i)A + m_iB \quad (4)$$

A deconvolution is performed for all 10 glasses simultaneously. A master spectrum is created combining all 10 ^{29}Si NMR resonances each shifted 60 ppm from the previous one in the direction of lower frequencies. Only signals in the range from −60 ppm to −120 ppm (original spectrum) are used. The deconvolution is then performed by subtracting the total ppm-shift from the $\delta(Q^4(0\mathrm{Al}))$ value for each resonance, for example, 2 × 60 ppm is subtracted from $\delta(Q^4(0\mathrm{Al}))$ of $C_{34}A_{11}S_{55}$, and 4 × 60 ppm is subtracted from $\delta(Q^4(0\mathrm{Al}))$ of $C_{43}A_{13}S_{44}$. The fitting procedure is performed by the scaled Levenberg−Marquardt algorithm, using reasonable starting values for the four unknown parameters, that is, $w = 8.5$ ppm (corresponding to FWHM = 10 ppm), $\delta(Q^4(0\mathrm{Al})) = -110$ ppm, $A = 7.5$ ppm, and $B = 5$ ppm. The validity of a model requires that the overall line shape of the ^{29}Si NMR resonance for each glass is matched by the deconvolution and that reasonable values for the four parameters are obtained.

(49) Greaves, G. N.; Meneau, F.; Kargl, F.; Wardi, D.; Holliman, P.; Albergamo, F. *J. Phys.: Condens. Matter* **2007**, *19*, 415102.

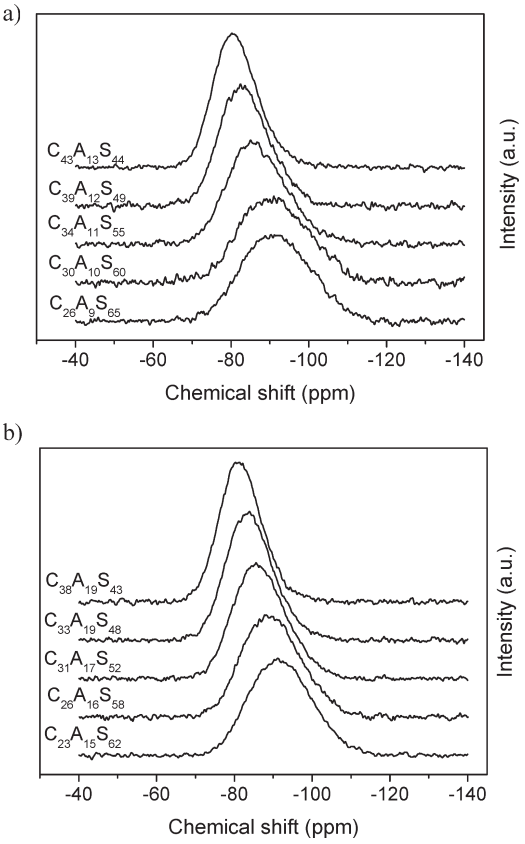

Figure 2. ^{29}Si MAS NMR spectra of the two series of calcium aluminosilicate glasses corresponding to the compositions (a) series 1, $C_{26}A_9S_{65}$ to $C_{43}A_{13}S_{44}$ and (b) series 2, $C_{23}A_{15}S_{62}$ to $C_{38}A_{19}S_{43}$. The spectra have been recorded under identical conditions at 7.05 T, using the spinning speed of ν_R = 7.0 kHz and a 120 s relaxation delay.

4. Results

4.1. ^{29}Si MAS NMR. Figure 2 shows the ^{29}Si MAS NMR spectra for the 10 glasses, each including a broad resonance with a line width (FWHM) ranging from 12.7 ppm ($C_{38}A_{19}S_{43}$) to 22.3 ppm ($C_{26}A_9S_{65}$). The resonances shift toward higher frequencies within each series, that is, $C_{26}A_9S_{65}$ to $C_{43}A_{13}S_{44}$ and $C_{23}A_{15}S_{62}$ to $C_{38}A_{19}S_{43}$, which reflects the increase in the content of both Ca_{excess} and Al. The resonance lineshapes and widths of the individual spectra are simulated using the deconvolution procedure described in section 3.5, to evaluate the models for the intermediate-range order in the glasses.

4.2. R-IRO Model. The predicted intensity distributions for the ^{29}Si subpeaks, obtained with the random IRO model, cannot be validated from simulations of the ^{29}Si MAS NMR spectra constraining the intensity of each subpeak to match the molar contents predicted in Table 3. The simultaneous deconvolution of all 10 ^{29}Si resonances provides a poor fit to the experimental data with a correlation coefficient of R^2 = 0.237, as illustrated in Figure 3 for $C_{26}A_9S_{65}$ to $C_{43}A_{13}S_{44}$. In addition, the resulting values of the four unknown fitting parameters, w = 29.5 ± 0.2 ppm, $\delta(Q^4(0Al))$ = 33 ± 1 ppm, A = −119 ± 1 ppm and B = −60 ± 1 ppm, are far from the expected values discussed in section 3.5. Figure 4 shows the distribution of subpeaks for the individual Si($Q^{ni}(m_iAl)$) units and the final description of the ^{29}Si resonances for

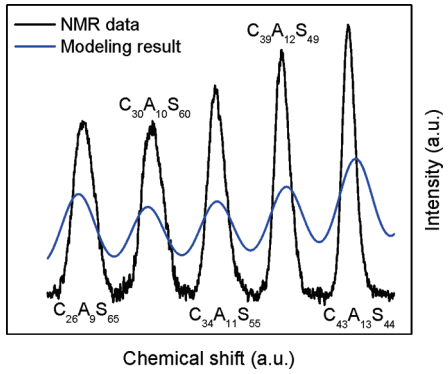

Figure 3. Result from simultaneous deconvolution of the resonances in all 10 ^{29}Si MAS NMR spectra using the R-IRO model, illustrated here for series 1, that is, $C_{26}A_9S_{65}$−$C_{43}A_{13}S_{44}$.

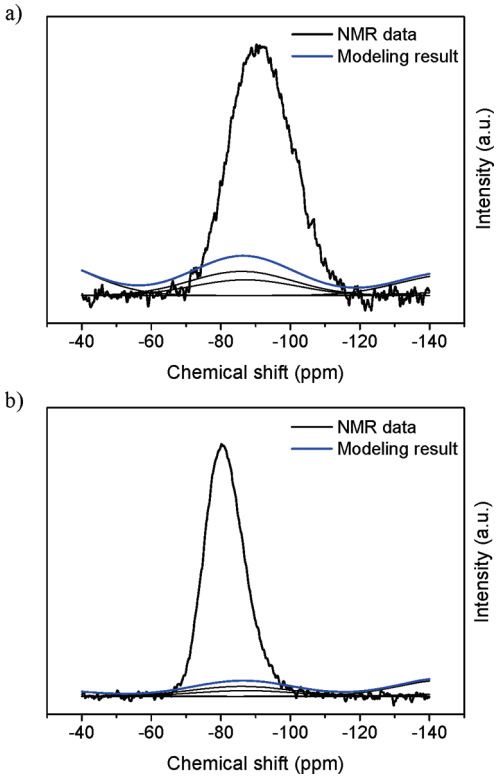

Figure 4. Deconvolution of the ^{29}Si NMR resonances for (a) $C_{26}A_9S_{65}$ and (b) $C_{43}A_{13}S_{44}$ using the R-IRO model. The experimental spectra are shown by thick black lines whereas the thin black lines illustrate the subpeaks originating from individual structural units. The sum of the deconvoluted resonances is shown by the blue line.

$C_{26}A_9S_{65}$ and $C_{43}A_{13}S_{44}$ from series 1. The difference between Figure 3 and 4 is because a large part of the intensity for the given sample is positioned outside the range of the experimental signal for that sample.

4.3. QH-IRO Model. When the intensities of the subpeaks are constrained to the contents of the different structural $Q^n(m\text{Al})$ units predicted by the quasi-heterogeneous IRO model, convincing agreements are achieved between the deconvoluted and experimental ^{29}Si MAS NMR spectra for all 10 glasses. This is illustrated in Figure 5 while the optimized values of the four unknown parameters (w, $\delta(Q^4(0Al))$, A, and B) are summarized in Table 5. Reasonable values of the four unknown parameters from eqs 3 and 4 are

Table 5. Optimized Parameters, w, $\delta(Q^4(0Al))$, A, and B, from Deconvolutions of the ^{29}Si MAS NMR Spectra Using the QH-IRO Model[a]

w (ppm)	FWHM[b] (ppm)	$\delta(Q^4(0Al))$ (ppm)	A (ppm)	B (ppm)	R^2
10.71 ± 0.03	12.61 ± 0.04	−100.75 ± 0.06	8.61 ± 0.04	3.92 ± 0.01	0.964

[a] The uncertainties are given as the standard deviations obtained from the fitting procedure. [b] FWHM is the full width at half-maximum, FWHM ≈ 1.18w.

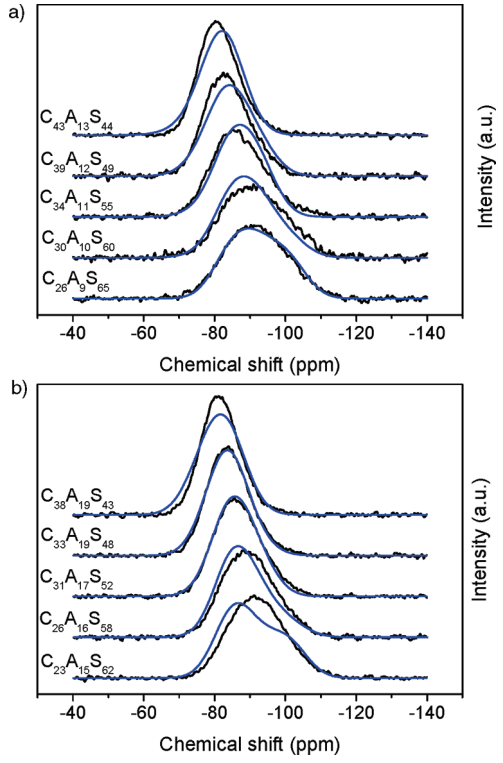

Figure 5. Deconvolutions of the ^{29}Si MAS NMR spectra for all glasses. The spectra are deconvoluted simultaneously using the QH-IRO model. The experimental spectra are shown by a black lines whereas the blue line illustrates the modeling result.

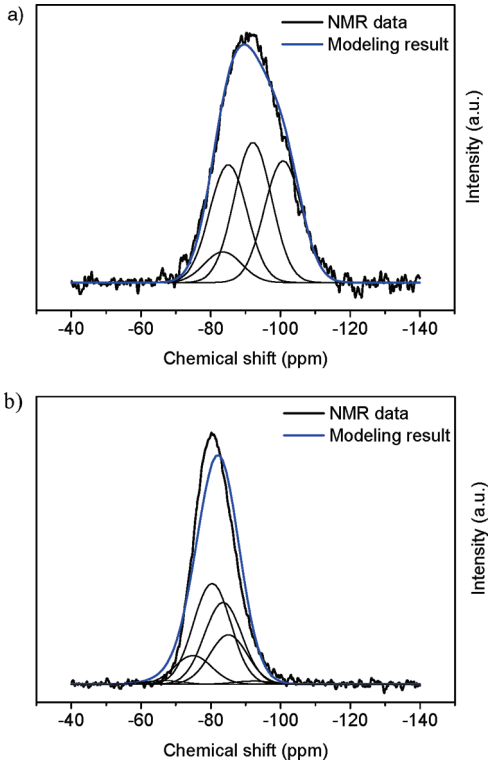

Figure 6. Deconvolution of the ^{29}Si NMR resonances for (a) $C_{26}A_9S_{65}$ and (b) $C_{43}A_{13}S_{44}$ using the QH-IRO model. The experimental spectra are shown by thick black lines whereas the thin black lines illustrate the subpeaks originating from individual structural units. The sum of the deconvoluted resonances is shown by the blue line.

obtained. The sum of the individual resonances provides an excellent fit to the experimental data, that is, $R^2 = 0.964$ for the simultaneous deconvolution of all 10 resonances.

The sensitivity of the optimized values for w, $\delta(Q^4(0Al))$, A, and B to the initial parameters used in the fitting procedure is tested. In this examination the starting values of w, A, and B are varied in the range ±50% of the original values, that is, $w = 8.5$ ppm, $A = 7.5$ ppm, and $B = 5$ ppm. The initial value for $\delta(Q^4(0Al))$ is varied in the range ±10% of the original shift, $\delta(Q^4(0Al)) = -110$ ppm. Different combinations of the starting values are used, for example, the largest value of $\delta(Q^4(0Al))$ ($\delta(Q^4(0Al)) = -120$ ppm) combined with the smallest values of A and B ($A = 3.75$ and $B = 2.5$) as the values of these parameters affect the result in opposite directions. The different combinations of starting values lead in all cases to values within the uncertainty limits of the parameters given in Table 5. Thus the parameters in Table 5 correspond to a strong local minimum obtained by the fitting procedure. In addition, the uncertainties associated with the four unknown parameters, given as the standard deviation obtained from the fitting procedure, are observed to be very small (i.e., ∼0.5% for A which shows the largest relative uncertainty). Thus, the analysis above shows that it is possible to obtain an excellent description of all 10 ^{29}Si resonances simultaneously, applying a structural model based on a quasi-heterogeneous IRO with just four unknown parameters which are determined with high precision (Table 5).

The individual descriptions of the resonances for each glass using the values of w, $\delta(Q^4(0Al))$, A, and B stated in Table 5 provide correlation coefficients (R^2) which range from 0.927 ($C_{23}A_{15}S_{62}$) to 0.996 ($C_{33}A_{19}S_{48}$) with an average of 0.970. Figure 6 shows the distribution of subpeaks for the individual Si($Q^{ni}(m_i\text{Al})$) units along with the final simulation of the ^{29}Si resonances for $C_{26}A_9S_{65}$ and $C_{43}A_{13}S_{44}$.

4.4. ^{27}Al MAS NMR. The ^{27}Al MAS NMR spectra (9.39 T) of the 10 glasses strongly suggest that Al is only present in tetrahedral coordination and mainly involved in Al−O−Si linkages, since the centerband resonances mainly cover the spectral range of tetrahedrally coordinated Al[50] with centers of gravity ranging from 45−52 ppm (Table 6). In addition, the ^{27}Al MAS NMR spectra of $C_{23}A_{15}S_{62}$ and $C_{38}A_{19}S_{43}$ recorded at 14.09 T (Figure 7) support these findings, since these spectra include similar centerband resonances, however, with smaller line widths (FWHM = 22.3 ppm for $C_{23}A_{15}S_{62}$ and FWHM = 21.8 ppm for $C_{38}A_{19}S_{43}$)

(50) Müller, D.; Gessner, W.; Behrens, H. J.; Scheler, G. *Chem. Phys. Lett.* **1981**, *70*, 59.

Table 6. Centers of Gravity and Line Widths Observed in the ^{27}Al and ^{29}Si MAS NMR Spectra and in the Simulated ^{29}Si NMR Spectra Using the QH-IRO Model

	$\delta_{cg}(^{27}Al)^a$ (ppm)	FWHM(^{27}Al)^a (ppm)	$\delta_{cg}(^{29}Si)^b$ (ppm)	FWHM(exp)^b (ppm)	δ_{cg}(QH-IRO)^c (ppm)	FWHM(QH-IRO)^c (ppm)
$C_{26}A_9S_{65}$	45.3	34.7	−92.4	22.3	−91.6	23.5
$C_{30}A_{10}S_{60}$	46.0	34.5	−90.9	23.1	−89.4	19.6
$C_{34}A_{11}S_{55}$	47.8	32.3	−87.4	17.7	−87.4	16.9
$C_{39}A_{12}S_{49}$	50.1	31.2	−84.0	15.4	−84.6	16.7
$C_{43}A_{13}S_{44}$	51.4	31.6	−81.6	13.3	−81.9	14.4
$C_{23}A_{15}S_{62}$	45.8	36.3	−91.8	19.2	−90.0	23.3
$C_{26}A_{16}S_{58}$	46.8	35.4	−89.5	18.4	−88.0	16.5
$C_{31}A_{17}S_{52}$	48.8	34.4	−86.6	15.9	−86.2	15.4
$C_{33}A_{19}S_{48}$	50.4	33.7	−84.0	13.9	−83.7	14.4
$C_{38}A_{19}S_{43}$	51.7	34.5	−81.6	12.7	−81.4	15.3

^{a} Center of gravity and line width of the centerband from the central transition observed in the ^{27}Al NMR spectra at 9.39 T. ^{b} Center of gravity and line width of the resonances observed in the ^{29}Si MAS NMR spectra (Figure 2). ^{c} Center of gravity and line width of the simulated ^{29}Si MAS NMR spectra obtained using the QH-IRO model (Figure 5).

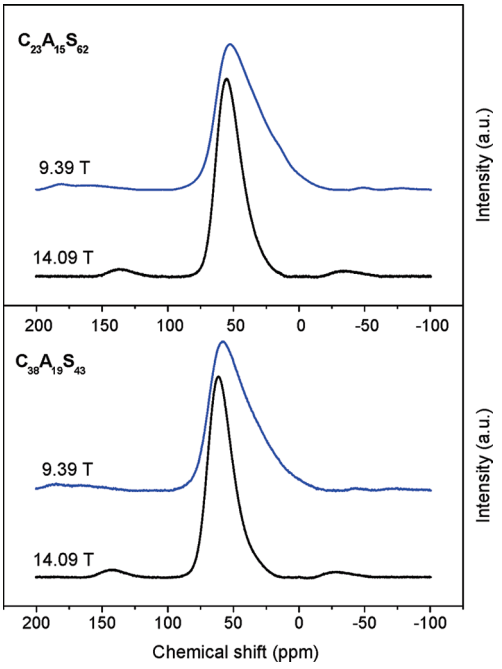

Figure 7. ^{27}Al MAS NMR spectra of $C_{23}A_{15}S_{62}$ and $C_{38}A_{19}S_{43}$ obtained at 9.39 and 14.09 T with spinning speeds of ν_R = 12.0 kHz and ν_R = 13.0 kHz, respectively.

and high-frequency shifts of the centers of gravity (δ_{cg} = 52.7 ppm for $C_{23}A_{15}S_{62}$ and δ_{cg} = 59.2 ppm for $C_{38}A_{19}S_{43}$) as compared to the resonances at 9.39 T. This reflects the inverse proportionality of the second-order quadrupolar broadening with the magnetic field strength. Isotropic chemical shifts from 55−65 ppm are characteristic for Al(OSi)$_4$ sites,[31,51,52] indicating that such sites are the dominant Al^{3+} environments in the glasses. Thus, these observations support the assumptions made in the modeling of the IRO of the calcium aluminosilicates.

For both series the centers of gravity for the ^{27}Al centerbands are observed to shift slightly toward higher frequency (Table 6 and Figure 7), indicating some changes in the local ^{27}Al environments. In analogy to the ^{29}Si chemical shifts, it is expected that the introduction of a NBO linked directly to Al induces a displacement of the chemical shift toward larger frequencies.[53] A similar effect on the ^{27}Al chemical shift is expected if Al−O−Al bonds replace Al−O−Si linkages.[31]

^{27}Al MQMAS NMR investigations of peralkaline CAS glasses with similar compositions as the glasses studied in this work have shown the presence of minor contents of 5-fold coordinated Al in the glasses[54,55] by the observation of AlO_5 contents of up to 7%. Thus, minor contents of AlO_5 are likely to be present in the glasses investigated in this work, despite no clear observations of these sites from the ^{27}Al NMR spectra in Figure 7 (the effect of these sites on the modeling is discussed later). In agreement with the conclusions drawn from Figure 7, no 6-fold coordinated Al is observed in the previous 27Al MQMAS NMR investigation.[54]

5. Discussion

5.1. Nature of the IRO. The ^{29}Si NMR resonances change systematically within each series of glasses (Figure 2), since the centers of gravity shift toward higher frequency and the line width decreases for the samples $C_{26}A_9S_{65}$−$C_{43}A_{13}S_{44}$ and $C_{23}A_{15}S_{62}$−$C_{38}A_{19}S_{43}$, respectively (Table 6). Consequently, the low-frequency edge of the resonances shifts from about −115 ppm to −100 ppm in the two series, indicating that the glasses $C_{39}A_{12}S_{49}$, $C_{43}A_{13}S_{44}$ and $C_{33}A_{19}S_{48}$, $C_{38}A_{19}S_{43}$ essentially do not contain any Si(Q^4(0Al)) units, which are the most shielded structural components with chemical shifts in the range −100 to −120 ppm.[22−24] According to the R-IRO model, Si(Q^4(0Al)) units are present in all 10 glasses although their content decreases along each series from $C_{26}A_9S_{65}$ to $C_{43}A_{13}S_{44}$ and from $C_{23}A_{15}S_{62}$ to $C_{38}A_{19}S_{43}$. Thus, this model is in contrast to the observed high-frequency shifts of the resonances in the above-mentioned series. The corresponding decrease in the FWHM values, observed experimentally within each series (Table 6), conflicts also with the R-IRO

(51) Müller, D.; Gessner, W.; Samoson, A.; Lippmaa, E.; Scheler, G. *J. Chem. Soc., Dalton Trans.* **1986**, 1277.
(52) Lippmaa, E.; Samoson, A.; Mägi, M. *J. Am. Chem. Soc.* **1986**, *108*, 1730.
(53) Müller, D.; Hoebbel, D.; Gessner, W. *Chem. Phys. Lett.* **1981**, *84*, 25.
(54) Neuville, D. R.; Cormier, L.; Massiot, D. *Chem. Geol.* **2006**, *229*, 173.
(55) Neuville, D. R.; Cormier, L.; Montoullout, V.; Massiot, D. *J. Non-Cryst. Solids* **2007**, *353*, 180.

model, which predicts an increasing number of non-negligible types of structural units as the contents of NBO and Al increases. These discrepancies demonstrate that the R-IRO model cannot describe the ^{29}Si MAS NMR spectra in a satisfactory manner.

The QH-IRO model predicts the presence of detectable contents of Si(Q^4(0Al)) units only for $C_{26}A_9S_{65}$, $C_{30}A_{10}S_{60}$, $C_{23}A_{15}S_{62}$, and $C_{26}A_{16}S_{58}$ whereas Si(Q^3(0Al)) units are the most shielded entities for the remaining glasses (except $C_{38}A_{19}S_{43}$) with an estimated chemical shift of −92.1 ppm. These predictions are in good agreement with the ^{29}Si MAS NMR spectra (Figure 2). In addition, the IRO hierarchy is capable of reproducing the experimentally observed decrease in FWHM within each series as indicated by the data in Table 6. The high-frequency edge of the ^{29}Si NMR resonances (roughly from −74 ppm to −67 ppm, Figure 2) is only shifted slightly toward higher frequency in the series $C_{26}A_9S_{65}$−$C_{43}A_{13}S_{44}$ and $C_{23}A_{15}S_{62}$−$C_{38}A_{19}S_{43}$ which may reflect the increasing content of Q^1(0Al) units (and Q^0 for $C_{43}A_{13}S_{44}$) predicted by the QH-IRO model (Table 4). These are the most deshielded structural units, and these species are present in all samples. In general, the Q^n(mAl) units corresponding to a low degree of condensation exhibit somewhat higher intensities for series 1 than series 2 in the QH-IRO model (Table 4) which is in accordance with the slightly lower center-of-gravity frequencies (δ_{cg}(^{29}Si)) observed for series 1 as compared to series 2 (Table 6). Thus, the distribution of structural units predicted from the QH-IRO model is found to approach the experimentally observed distribution and thereby, the QH-IRO model provides a suitable description of the intermediate range order in the CAS glasses, despite small variations between the predicted and the experimental results (Figure 5). The variations between the modeling results and the experimental ^{29}Si NMR resonances may be explained by the strict division between depolymerized calcium silicate regions and highly polymerized regions of alternating SiO_4-($^1/_2$Ca)AlO_4 units used within the modeling. This very strict division will most likely not be fully retained in the glasses. For example, minor contents of Al can be expected within the depolymerized regions and the 1:1 ratio between Si and Al in the highly polymerized regions is possibly violated to some extent.

Engelhardt et al[56] have investigated the structure of a wide range of CAS compositions, using a similar approach as employed in the present study, and described the structure in terms of a distribution of Si(Q^n(mAl)) structural units. In their work, the applicability of a model also assuming Al to be linked preferentially to the most polymerized Si(Q^n) units is tested and found to provide a reasonable description of the experimental data. This supports the quasi-heterogeneous distribution of Al in the second coordination sphere of Si found in the present study.

Figure 8 illustrates a schematic representation of the intermediate-range structure predicted from the two

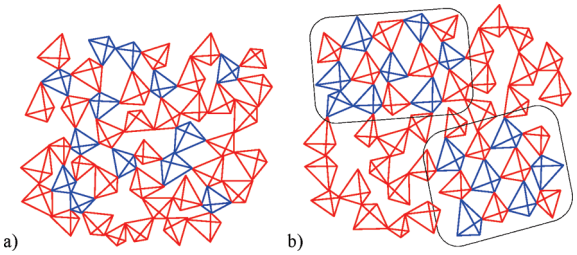

Figure 8. Schematic representations of the intermediate-range structure of the CAS glasses projected into two dimensions. Only the network forming tetrahedra are shown in the figure. Oxygen is located in the four corners of the tetrahedron surrounding the cation. The red tetrahedra indicate SiO_4 units and the blue tetrahedra represent the ($^1/_2$Ca)AlO_4 units. Part (a) illustrates a structural arrangement following the random IRO model while (b) visualizes the hierarchy in the IRO predicted by the quasi-heterogeneous IRO model. The highly polymerized regions of alternating SiO_4 and ($^1/_2$Ca)AlO_4 units are marked by squares.

modeling approaches. The content of intermediate-range clustering regions is expected to increase in each series as the contents of both Al and NBO increase. Thus, the hierarchy in the intermediate-range order and the degree of heterogeneity increases within each series of glasses, that is, $C_{26}A_9S_{65}$ to $C_{43}A_{13}S_{44}$ and from $C_{23}A_{15}S_{62}$ to $C_{38}A_{19}S_{43}$.

5.2. Structural Role of Al. Both theoretical models, describing the spatial arrangement of structural units in the intermediate range, are based on the distribution of Al around Si and focus only on the identity of the first and second nearest neighbors of Si. For these approaches the fulfillment of the Al avoidance principle within the framework depends on the Si/Al ratio and the content of NBOs bound to Si. It is possible to fulfill the Al avoidance principle for all glasses except $C_{38}A_{19}S_{43}$, if it is assumed that Al is only present as Al(Q^4) units. For $C_{38}A_{19}S_{43}$ at least 17% of Al is expected to be in Al−O−Al linkages.

The content of Al−O−Al linkages depends also on the specific model. For example, the random IRO model does not contain any assumption regarding the Al avoidance principle since it is only assumed that no clustering of Al occurs. In the R-IRO model (Table 3) the individual structural units must be accommodated into one continuous network to form the glass, which provides further limits on the Al avoidance as considerable contents of Si−O−Si bonds are predicted. Using the R-IRO model at least 32% of Al in $C_{26}A_9S_{65}$ take part in Al−O−Al linkages increasing to 58% for $C_{43}A_{13}S_{44}$. For series 2 the fraction of Al in Al−O−Al linkages is at least 42% for $C_{23}A_{15}S_{62}$ and 60% for $C_{38}A_{19}S_{43}$. Thus, about 50% of the Al is expected in Al−O−Al linkages, in agreement with the random nature of the modeling approach. However, these fractions of Al in Al−O−Al linkages appear unrealistically high since they are significantly larger than those reported for "charge compensated" CAS systems.[10,14]

In the QH-IRO model an alternating SiO_4−AlO_4 structure is assumed within the highly polymerized Al-containing regions, thus having a Si/Al ratio of 1:1. This means that the Al avoidance principle breaks down when Al is assigned to Si(Q^3), that is, Si associated with only 3 BO. For $C_{26}A_9S_{65}$, $C_{30}A_{10}S_{60}$, $C_{23}A_{15}S_{62}$, and $C_{26}A_{16}S_{58}$

(56) Engelhardt, G.; Nofz, M.; Forkel, K.; Wihsmann, F. G.; Magi, M.; Samoson, A.; Lippmaa, E. *Phys. Chem. Glasses* **1985**, *26*, 157.

no Al−O−Al linkages are expected since all Al sites are assigned to fully polymerized SiO_4 units. For $C_{34}A_{11}S_{55}$, $C_{39}A_{12}S_{49}$, and $C_{43}A_{13}S_{44}$, the expected fractions of Al in Al−O−Al linkages are 1%, 10%, and 17%, respectively. In series 2, the expected contents of Al in Al−O−Al linkages are 3%, 10%, 19% for $C_{31}A_{17}S_{52}$, $C_{33}A_{19}S_{48}$, and $C_{38}A_{19}S_{43}$, respectively. These degrees of Al avoidance are in the same range as those reported previously for the "charge compensated" CAS systems.[10,14]

As mentioned in section 4.4, the observed shifts in $\delta_{cg}(^{27}Al)$ (Table 6) indicate changes in the local ^{27}Al environment. The high-frequency shift of the resonances within each series may reflect an increase in the content of Al−O−Al linkages as predicted from both models.[31] However, the rather small displacements in centers of gravity (Table 6) seem not large enough to justify the presence of 50% Al in Al−O−Al linkages, which further supports the suitability of the quasi-heterogeneous model in the description of IRO in the CAS system.

The assumption that Al is solely present in tetrahedral coordination seems a good first approximation as this is clearly the dominant structural arrangement for the aluminate species. However, the presence of minor contents of 5-fold coordinated Al (< 7%) is expected to affect the modeling result. So far, the structural role of 5-fold coordinated Al is not fully understood, and it is unclear whether penta-coordinated Al can be regarded as a network former or as a modifying component.[54,55] To charge balance an AlO_5 units an additional positive charge is required as compared to Al in tetrahedral coordination. In this situation the actual content of Ca_{excess} will be lower than assumed in the modeling. This can possibly explain why the high-frequency edge for the majority of the modeling results in Figure 5 is positioned at slightly higher frequencies than the experimental data.

5.3. Variations of the Fitting Parameters. The fitting procedure employs a constant value to describe the dependence of $\delta(^{29}Si)$ on the introduction of NBO, that is, the fitting parameter A. Thus, the displacement of the chemical shift is the same for the introduction of the first NBO as, for example, for the third one. On the basis of comprehensive studies of silicate minerals with different degrees of polymerization, ^{29}Si chemical shift ranges for the different types of Q^n units have been reported.[22−24] Furthermore, from structural modeling of about 50 CAS glasses within a wide compositional range, chemical shifts for the Q^n units have been given by Engelhardt et al.[56] Considering the mean values of each interval combined with the results of Engelhardt et al., a linear regression of these data results in the value for A of 9.6 ± 0.9 ppm.

A similar approach is used to describe the dependency on $\delta(^{29}Si)$ on the replacement of a Si−O−Si by a Si−O−Al bond. From studies of aluminosilicate minerals with zeolite-like compositions, ranges of $\delta(^{29}Si)$ are obtained for the different $Q^4(m\text{Al})$ units.[8,24] The reported ranges suggest that the introduction of one Al in the second coordination sphere results in a displacement of the chemical shift of (6.6 ± 0.3) ppm. Thus, the displacement can be regarded as independent of the number of Al already introduced within the second coordination sphere of the $Si(Q^4)$ units. However, the absolute values for B found in the previous studies are larger than the B values obtained in this study. This reflects most likely the significant content of depolymerized structural units (Q^n with $n < 4$) present within the glasses of this work. This observation is consistent with the results obtained by spectral editing in ^{29}Si MAS NMR spectra of glasses with anorthite composition.[57] Likewise, variations in the Si/Al ratio are expected to affect the values of both A and B.

The line width of all subpeaks, originating from the different structural units, is during the modeling procedure regarded as a constant parameter. Of course, this is an assumption, as the width is known to depend on both the topological, that is, the distribution of bond angles and distances, and chemical environment of Si. The similar cooling rates, used during the preparation of all 10 glasses, ensure similar bond-angle and atomic distance distributions for all glasses. Thus, it is reasonable to assume that the broadening because of bond-angle and atomic distance disorder is constant for all samples. In a previous study of two series of aluminosilicates glasses on the meta-aluminous limit, the widths of the individual $Si(Q^4(m\text{Al}))$ resonances have been determined by modeling of ^{29}Si MAS NMR resonances.[8] For calcium aluminosilicates, FWHM is reported to vary in the range 0.8−1 ppm among the various $Si(Q^4(m\text{Al}))$ units, whereas for sodium aluminosilicates, the variation in FWHM is found to be ∼2 ppm. The observed variations are not systematic which makes it difficult to incorporate them into the modeling procedure. In addition, the line broadening because of topological disorder diminishes the relative variation of FWHM. The absolute values for FWHM found in previous studies[8,57] (FWHM = 11−13 ppm) is comparable to the results obtained in the present work.

Further improvements of the description of the parameters A, B, and FWHM may, of course, provide more sophisticated modeling procedures and thereby potentially further improve the agreement with experimental data.

5.4. Impact of Structural Heterogeneity on Properties. The viscous behavior and crystallization tendency for the 10 CAS compositions studied in this work have been investigated recently[19] with the aim of finding the optimal composition of glass particles for the potential use as supplementary cementitious materials in blends with Portland cement. In that study it was found that both series only exhibit a weak dependence of the composition on the fragility but a strong compositional dependence of the stability of the glasses toward crystallization during reheating.[19] The melt workability and glass stability affect the applicability of the glasses in technical applications. Thus, it is of special interest to understand correlations between compositional changes and changes in structure and properties.

The observed intermediate-range quasi-heterogeneity, which is characterized by the clustering of highly

(57) Hiet, J.; Deschamps, M.; Pellerin, N.; Fayon, F. *Phys. Chem. Chem. Phys.* **2009**, *11*, 6935.

depolymerized SiO_4 units and highly polymerized AlO_4 and SiO_4 tetrahedra, is expected to influence the physical properties of the 10 CAS glasses and melts. In general, the glasses in series 1 show a larger stability toward crystallization upon reheating as compared to the glasses in series 2. In particular $C_{26}A_9S_{65}$ and $C_{30}A_{10}S_{60}$ exhibit superior stability[19] which may be explained by the observed hierarchy in IRO. The compositions in series 2 have the highest content of Al and for this reason the number of highly polymerized clusters of alternating SiO_4–($^1/_2$Ca)-AlO_4 units is larger for series 2 as compared to series 1. These cluster regions in the IRO are expected to be frozen in at viscosities of $\eta \approx 10^4$ Pa·s.[39,43] Thus, they will remain in the glass structure during reheating until temperatures markedly above the glass transition are reached. These cluster regions constitute inhomogeneities capable of inducing heterogeneous nucleation. Large numbers of inhomogeneities create the largest reduction of the energy barrier toward crystallization. Another possibility is that clusters exceeding the critical sizes can act as nuclei for the crystallization process. The identity of the crystalline phases formed during heating of the glasses has been determined by powder X-ray diffraction for series 1.[58] Prior to these investigations, the glasses were subjected to a dynamic heating to 1523 at 20 K/min. No crystalline phases are observed in $C_{26}A_9S_{65}$ and $C_{30}A_{10}S_{60}$, whereas crystals are detected in the remaining glasses of series 1, the principal crystalline phases being anorthite, wollastonite, and pseudowollastonite. The composition of anorthite ($CaAl_2Si_2O_8$) corresponds to that expected for the highly polymerized regions of alternating SiO_4 and ($^1/_2$Ca)AlO_4 tetrahedra, whereas the composition of wollastonite and pseudowollastonite ($CaSiO_3$) corresponds to that expected for intermediate-range SiO_4 clusters rich in NBOs. For $C_{43}A_{13}S_{44}$, approximately 10% of the crystals are identified as gehlenite ($Ca_2Al[AlSiO_7]$). This phase is expected to be formed from clusters rich in Al. Thus, the formation of gehlenite in $C_{43}A_{13}S_{44}$ also indicates the breakdown of the Al avoidance principle. A study on the dependence of crystallization on the degree of undercooling for a series of calcium aluminosilicate liquids in the same compositional range as studied in this work also reveals the formation of non-isochemical crystal phases that reflects compositional fluctuations, and hence, structural heterogeneities in the melts. The phases reflecting compositional fluctuations form at low temperatures at which the mobility of the ions is restricted.[59]

Fragility is a measure of the deviation of the melt flow behavior from Arrhenian behavior.[60] A fragile melt exhibit non-Arrhenian behavior, whereas a strong melt has a near-Arrhenian behavior. The fragility reflects the degree of order in a melt where a strong melt generally has a high degree of short-range order while fragile melts do not have well-defined short-range order.[60] The strongest melt known today is pure SiO_2 and addition of a network modifying cation (e.g., Ca) into pure SiO_2 increases the disorder and thus the fragility. The fragility of aluminosilicates is also influenced by the Al content and it has been reported that the fragility of peralkaline CAS melts increases with a decreasing Si/Al ratio.[61] Thus, the fragility is expected to increase within each series of glasses from $C_{26}A_9S_{65}$ to $C_{43}A_{13}S_{44}$ and from $C_{23}A_{15}S_{62}$ to $C_{38}A_{19}S_{43}$, since both the content of NBO and Al increase in these series. However, only a minor compositional dependence of the melt fragility was observed in our recent study,[19] which may reflect the increasing degree of quasi-heterogeneity in the intermediate-range. This increase in IRO may counterbalance the expected increasing short-range disorder as the contents of NBO and Al increase. Thus, the quasi-heterogeneous nature of the IRO may in general account for the compositional dependence of stability of the glasses toward crystallization and fragility as observed for the 10 melts in the CAS system.

5.4. Perspective. As proved above, the nature of the intermediate-range order in CAS glasses is not random. Instead the appearance of the ^{29}Si MAS NMR resonances gives evidence of chemical fluctuations in the intermediate-range of the glass structure. These fluctuations can be described as clustering of highly depolymerized CaO-SiO_2 containing regions and highly polymerized regions of alternating SiO_4 and AlO_4 tetrahedra. Figure 5 shows the good agreement of this quasi-heterogeneous modeling with the experimental results obtained by ^{29}Si NMR. Although the modeling is found to provide a convincing description of the data, minor deviations between the simulated and experimental resonances are observed (Figure 5). To reduce these deviations, future models may consider the following refinements. (i) The content of five-coordinated Al may be probed by ^{27}Al MQMAS NMR and subsequently considered in the modeling approach. (ii) Ab initio calculations of the NMR parameters may be a promising approach, which can potentially be used to estimate influence of the fitting parameters, for example, the width, on variations in chemical and structural environments for the various structural units. (iii) The approach used in this work for obtaining structural information may potentially be combined with other methods, particularly, molecular dynamic simulations,[62] to provide new insight about the local structure of the glasses.

6. Conclusions

In this work, the intermediate-range order (IRO) for 10 peralkaline CAS glasses has been investigated by ^{29}Si MAS NMR in combination with structural modeling. Two approaches for the IRO have been established within the framework of the continuous random network and modified random network models, respectively. The first approach, that is, the R-IRO model, employs a random

(58) Moesgaard, M., unpublished data.
(59) Roskosz, M.; Toplis, M. T.; Richet, P. *J. Non-Cryst. Solids* **2006**, *352*, 180.
(60) Angell, A. *J. Non-Cryst. Solids* **1991**, *131*–*133*, 13.
(61) Solvang, M.; Yue, Y. Z.; Jensen, S. L.; Dingwell, D. B. *J. Non-Cryst. Solids* **2004**, *336*, 179.
(62) Vargheese, K. D.; Tandia, A.; Mauro, J. C. *J. Chem. Phys.* **2010**, *132*, 194501.

spatial arrangement of Al within the second coordination sphere to Si whereas the key factor of the second model, that is, the QH-IRO model, is the clustering of regions rich in highly polymerized AlO_4 and SiO_4 units and other regions rich in highly depolymerized SiO_4 units. This clustering is described as a hierarchy in the IRO. The applicability of the two modeling approaches to describe the structure of the peralkaline CAS glasses has been examined by deconvolution of experimental ^{29}Si MAS NMR spectra using subpeaks for the different structural units with relative intensities predicted from the models. The quasi-heterogeneous modeling approach, emphasizing a hierarchy in the IRO, results in good agreements between the simulated and experimental ^{29}Si MAS NMR spectra for all 10 glasses. In contrast, the random modeling approach is not capable of reproducing the ^{29}Si NMR resonances in a satisfactory manner. Thus, the structure of the glasses studied in the present work is dictated by a quasi-heterogonous IRO. Furthermore, the IRO hierarchy approach may explain the compositional dependences of the glass stability against crystallization, the glass forming ability and the fragility for the 10 glass systems.

Acknowledgment. The Danish National Advanced Technology Foundation is acknowledged for financial support. We thank Duncan Herfort and Lise Frank Kirkegaard (Aalborg Portland A/S, Denmark) for experimental assistance with the wet chemical analyses of the glasses. John Mauro (Corning Incorporated, NY, USA) is thanked for useful discussion. The use of the facilities at the Instrument Centre for Solid-State NMR Spectroscopy, Aarhus University, sponsored by the Danish Natural Science Research Council, the Danish Technical Science Research Council, Teknologi-styrelsen, Carlsbergfondet, and Direktør Ib Henriksens Fond, is acknowledged.